

Particle swarm optimization of silicon photonic crystal waveguide transition

RYO SHIRATORI, MASAYA NAKATA, KOSUKE HAYASHI, TOSHIHIKO BABA*

Department of Electrical and Computer Engineering, Yokohama National University, 79-5 Tokiwadai, Hodogayaku, Yokohama 240-8501, Japan

*Corresponding author: baba-toshihiko-zm@ynu.ac.jp

Received XX Month XXXX; revised XX Month, XXXX; accepted XX Month XXXX; posted XX Month XXXX (Doc. ID XXXXX); published XX Month XXXX

Slow light generated through silicon (Si) photonic crystal waveguides (PCWs) is useful for improving the performance of Si photonic devices. However, the accumulation of coupling loss between a PCW and Si optical wiring waveguides is a problem when slow light devices are connected in series in a photonic integrated circuit. Previously, we reported a tapered transition structure between these waveguides and observed a coupling loss of 0.46 dB per transition. This current study employed particle swarm optimization to engineer the arrangement of photonic crystal holes to reduce loss and succeeded in demonstrating theoretical loss value of 0.12 dB on average in the wavelength range of 1540–1560 nm and an experimental one of 0.21 dB. Crucially, this structure enhances the versatility of slow light. © 2021 Optical Society of America

<http://dx.doi.org/10.1364/OL.99.099999>

Silicon (Si) photonic platforms allow the fabrication of small, low-loss optical devices and large-scale, high-density photonic integrated circuits. Complementary metal-oxide-semiconductor (CMOS) processes provide low-cost and high-volume production. However, the established structures and fabrication processes of the basic components mean achieving significant improvements in performance is difficult. To solve this constraint, slow light has been studied to further improve their performance owing to enhanced light-matter interactions [1]. Photonic crystal waveguides (PCWs), which consist of a waveguide channel sandwiched by hole arrays, can be fabricated in a standard CMOS process and generate slow light on-chip. In particular, dispersion-engineered PCWs [2] generate wideband, low-dispersion slow light, which has been applied to nonlinear enhancement [3, 4], delay and dispersion tuning [5], optical correlation [6], high-speed modulation [7], and beam scanning [8].

Simple Si channel waveguides are usually used for optical wiring, and PCWs are inserted into functional parts; however, boundaries between these waveguides can lead to coupling losses due to mode mismatches. The suppression of this loss is crucial to enhancing the versatility of PCWs. For this purpose, alternative transition structures have been investigated for air-clad PCWs, e.g.,

modulations in hole diameter [9, 10] and lattice constant [11], tapered structures [12, 13], and edge structure adjustment [14]. These were all based on two-dimensional calculations that lacked the consideration of out-of-plane scattering losses. Furthermore, practical applications of PCW require a robust silica cladding with greater light line limitations than those for air cladding, meaning optimization is not necessarily analogous. Previously, we applied a tapered structure to a silica-clad PCW, as shown in Fig. 1, where the slow light photonic band temporarily crosses the silica light line in the taper [15]. The taper length and edge widths were designed by full three-dimensional (3D) calculations, and a coupling loss of 0.46 dB was determined experimentally; however, this means that nearly 1 dB of loss occurs solely by inserting a PCW, which may restrict their use at multiple points in a circuit.

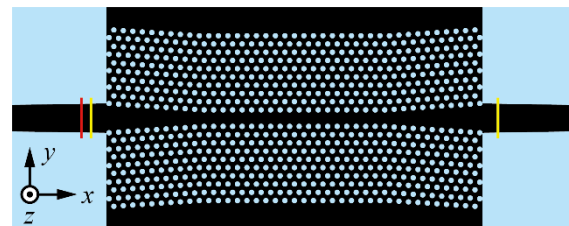


Fig. 1 Schematic of tapered transition structure between a Si waveguide and PCW. Red and yellow lines indicate the position of the excitation and monitors, respectively, in our models.

In this study, we achieved a practical low loss by optimizing the hole positions of the first three rows and 10 lines at the transition. Even assuming the PCW to be symmetrical, the number of target holes is 30; thus, the number of parameters is as large as 60 for the xy position shifts. Recently, to cope with the design complexity of such photonic devices, machine learning and related optimization techniques have been implemented [16–20]. In this study, we employed particle swarm optimization (PSO) [21], an iterative process of optimization using repetitive computational generations, and finally obtained a structure with theoretical and experimental loss values of 0.12 and 0.21 dB, respectively.

The PCW consists of triangular lattice hole arrays in a Si slab, a single-row line defect waveguide core, and silica cladding with a third-row shift making the slow-light spectrum wider and its group

velocity dispersion lower, which we call lattice-shifted PCW (LSPCW) [5–8]. The parameters were set at a Si slab thickness of 210 nm, hole diameter of 192 nm, lattice constant of 394 nm, lattice shift of 95 nm, and waveguide length of 50 cycles of the lattice constant (19.3 μm) to achieve a slow light group index of ~ 20 and a flat band spectral width of ~ 20 nm for the transverse-electric polarization around the wavelength ($\lambda = 1550$ nm). As an initial structure, a slow taper of 10 cycles was assumed to linearly widen the line defect toward the edge. The outer rows of holes were moved outward according to the widening of the line defect so that the edge width was 1002 nm, with the Si waveguide having the same width at the transition. Although this width is not single modal, it can be quasi single modal when the width is narrowed to < 500 nm through an adiabatic taper. A commercial software package (Lumerical FDTD Solutions) with a refractive index library ($n_{\text{Si}} = 3.4784$, $n_{\text{silica}} = 1.44427$) and 20 personal computers (Intel Core i7-6700) were used to perform the 3D finite difference time domain simulation of light propagation. The red and yellow lines in Fig. 1 show the positions of an excitation source and monitors, respectively, and the transmission spectrum was obtained from the ratios of the monitor values. To eliminate the influence of small, uncoupled components from the excitation source on the Si waveguide mode, the obtained spectrum was divided by the spectrum calculated for a straight Si waveguide of the same width and length, and the coupling loss was considered to be half of the transmission loss.

PSO is a search algorithm that finds optimal solutions to special problems by stochastically moving multiple computational particles that have position and velocity vectors of the same dimension as the input parameters'. This study employed a speed-constrained multi-objective PSO algorithm [22], which avoids early convergence to a local solution by limiting speed and thereby enhancing the possibility of reaching the global best solution in multi-objective optimization. Starting from the above initial structure, we generated 100 models in which 30 holes were moved randomly within ± 30 nm of the xy directions during the first generation. We then calculated the transmission spectrum and evaluated the average loss in the $\lambda = 1540$ – 1560 nm range, which is a standard working spectrum for the LSPCW assumed. We also evaluated the spectral width ($\Delta\lambda$) that achieved a coupling loss of ≤ 0.5 dB (an example value of low loss) to avoid a situation that PSO seeks a solution giving a particularly low loss at a narrow $\Delta\lambda$. We found Pareto solutions that balanced these two requirements. The next 100 models were calculated by adding a velocity vector toward the Pareto solutions and a random velocity vector to each of the previous models. To save computation time, we initially selected accuracy 1 in the above software (lowest accuracy level), which resulted in a calculation time for a time step of 36,689 (equivalent to 5 ps) of approximately 280 s. We repeated this process for 200 generations. Figure 2 shows the evolution of the loss and $\Delta\lambda$ of 30 models, showing that the loss decreased while the $\Delta\lambda$ increased as the generations progressed. The optimal solution was nearly reached by the fifth generation, and by the 20th generation the results were almost saturated. Then, using the best structure and improving the accuracy (accuracy 4), we calculated an updated loss of 0.12 dB and $\Delta\lambda$ of 35 nm, which required ~ 3 h computation time for a time step of 109,587 (equivalent to 5 ps). This broad $\Delta\lambda$ might be due to the underestimation of out-of-plane radiation losses above the light line in the short LSPCW model.

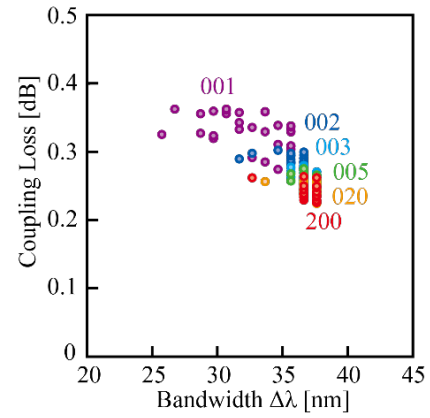


Fig. 2 Evolution of coupling loss averaged for $\lambda = 1540$ – 1560 nm and spectral width giving a loss of ≤ 0.5 dB, calculated for 30 models at different generations of PSO, denoted by numbers in the figure. The lowest accuracy setting was used (accuracy 1).

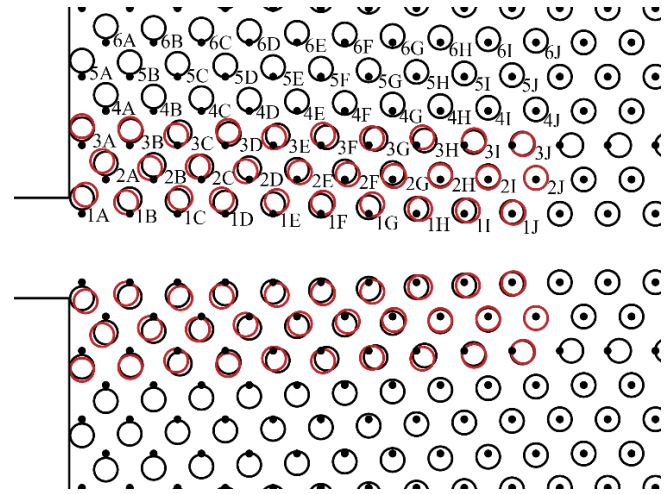


Fig. 3 Detail of the best transition structure. Black dots show the center position of holes in a simple single-row line defect PCW with no taper or shifts. Black and red circles show the initial tapered structure and the best structure after optimization, respectively.

Table 1 x and y shifts in the position of holes between the best structure and a simple single-row line defect PCW in nm. Symbols correspond to those in Figure 3. Beyond row J is the standard LSPCW.

Row	A	B	C	D	E	F	G	H	I	J
1	x	30	-30	24	-30	30	18	30	30	12
	y	190	114	158	142	126	110	94	48	10
2	x	-30	-30	-30	-30	24	24	12	0	0
	y	184	114	128	82	72	50	34	36	20
3	x	0	4	-11	23	8	18	27	49	82
	y	190	162	98	142	78	104	70	78	50
4	x	0	0	0	0	0	0	0	0	0
	y	160	144	128	112	96	80	64	48	32
5	x	0	0	0	0	0	0	0	0	0
	y	160	144	128	112	96	80	64	48	32
6	x	0	0	0	0	0	0	0	0	0
	y	160	144	128	112	96	80	64	48	32

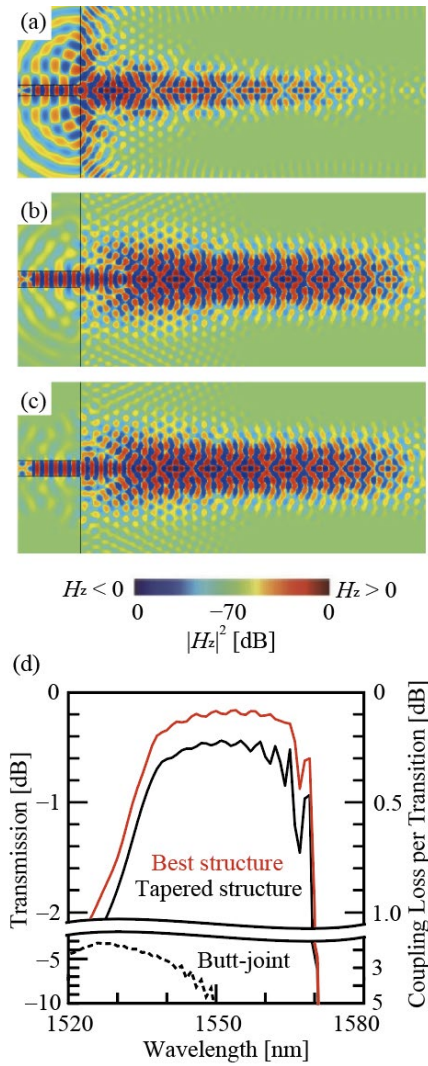


Fig. 4 Light transmission results from the high accuracy setting (accuracy 4) showing modal magnetic field intensity distributions $|H_z|^2$ at $\lambda = 1.55 \mu\text{m}$ for (a) butt-joint, (b) simple tapered, and (c) best structures. (d) Transmission spectra for (b) and (c). The coupling loss per transition on the right axis is obtained by halving the transmission.

Figure 3 shows the optimal transition structure following optimization, with the black and red circles depicting the holes of the simple tapered structure and best structure, respectively. Table 1 also shows the center coordinates of each hole in the best structure. In the first row, the best structure is characterized by an outward shift in 1A, an inward shift in 1B, and an outward shift in 1C–G, which then gradually converges to a simple taper. Such modifications may initiate the repeated expanding and shrinking behaviors of slow-light mode, which is usually observed in photonic crystal waveguides. Figure 4(a)–(c) compares the modal intensity of a butt-joint structure, the simple tapered structure, and the best structure in a wide dynamic range of 70 dB. The butt-joint structure shows strong reflection at the boundary, while reflection is suppressed in the tapered structure and particularly suppressed in the best structure. Figure 4(d) compares the corresponding transmission spectra. Averaged over the $\lambda = 1540\text{--}1560 \text{ nm}$ range for the butt-joint, simple tapered and best structures, the coupling losses are >10 , 0.30 and 0.12 dB, respectively.

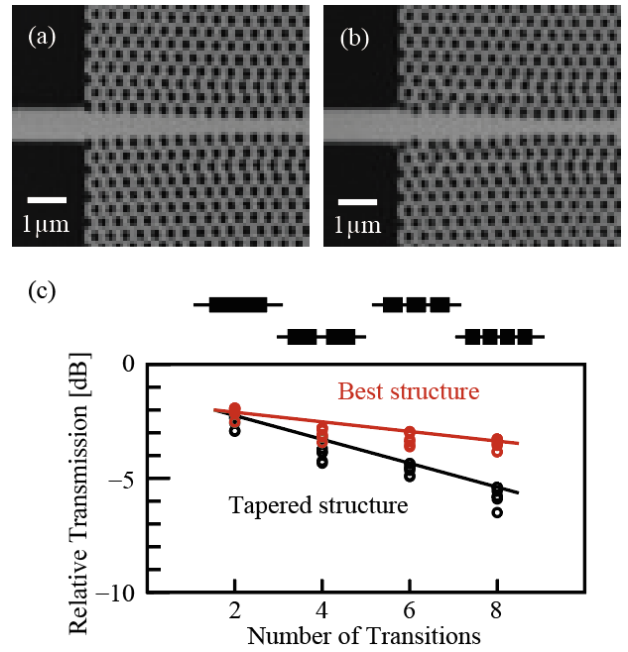


Fig. 5 Experimental results. (a), (b) Confocal laser microscope images of fabricated simple tapered structure and best structure, respectively. (c) Transmission intensity with the number of divisions, where the intensity for the same length Si waveguide was used as a reference. Upper symbols depict the schematic of divided LSPCWs.

A Si photonics CMOS process utilizing a 200 mm diameter silicon-on-insulator (Si layer thickness of 210 nm), stepper exposure krypton fluoride excimer laser ($\lambda = 248 \text{ nm}$), and phase shift mask were used to fabricate the device. The process resolution was approximately 110 nm. However, the grid size of the photomask was 1 nm, and the positioning resolution was 0.25 nm after $4\times$ reduction projection exposure. Therefore, the small position shifts of holes shown in Table 1 were sufficiently reproducible. Figure 5(a) and (b) show confocal laser microscopy images of the two types of fabricated device. Compared with the smooth arrangement of the simple tapered structure, the modifications of the best structure appear to be rather irregular. Measurements of the light input and output between the external optical fibers and singlemode 400-nm-wide Si waveguides were carried out using spot size converters. The Si waveguides were widened through a $50\text{-}\mu\text{m}$ -long linear slow taper and connected to the transition of an LSPCW of $800 \mu\text{m}$ total length. On the same chip, different devices were also fabricated, in which the LSPCW was divided two, three, or four times, maintaining the LSPCW's total length, and a Si waveguide was inserted between each segment for a total transition number of 2, 4, 6, or 8. The transmission intensity was measured using an amplified spontaneous emission source and was automatically averaged in the wavelength range defined by an incorporated band-pass filter. This helped to stabilize the optical alignment for each sample. Figure 5(c) shows the variation in transmission intensity corresponding to the number of transitions, which were measured for five different chips at various locations in the wafer and normalized against the intensity for the Si waveguide without the LSPCW. From the gradient obtained by the least mean square for the highest transmission data of each number of transitions, the coupling loss values were determined to be 0.52 and 0.21 dB, respectively, for the simple taper and best structures. The latter

value shows improvement by the PSO optimization, while it is higher than the calculated value. One candidate reason is the repeated use of Si waveguide tapers, but the increase by 0.09 dB is too large. Another reason considered is that some arranged holes are too close so that their shapes are deformed slightly. We calculated a lower loss of 0.09 dB for another hole arrangement with narrower local hole spacings and showed a higher loss of 0.5 dB in the experiment. The intercept of 1.0–1.5 dB in Fig. 5(c) indicates excess loss from the LSPCW, for which the propagation loss is estimated to be 12–19 dB/cm. The separately measured group index ranged from 20 to 25.

In conclusion, the transition structure between the slow light PCW and Si waveguide was optimized by applying a PSO multi-objective algorithm. Theoretical and experimental practical low losses of 0.12 and 0.21 dB, respectively, were determined, which greatly enhance the versatility of slow light. This work proves the usefulness of informatic technology to Si photonics and photonic crystals, and similar optimizations are expected to improve the performance of various photonic devices.

Funding. New Energy and Industrial Technology Development Organization (NEDO) (project #13004); Accelerated Innovation Research Initiative Turning Top Science and Ideas into High-Impact Values (ACCEL) (JPMJAC1603).

Disclosures. The authors declare no conflicts of interest related to this article.

Data availability. Data underlying the results presented in this paper are not publicly available at this time but may be obtained from the authors upon reasonable request.

References

1. T. F. Krauss, *Nat. Photonics* **2**, 448 (2008).
2. T. Baba, *Nat. Photonics* **2**, 465 (2008).
3. B. Corcoran, C. Monat, C. Grillet, D. J. Moss, B. J. Eggleton, T. P. White, L. O'Faolain and T. F. Krauss, *Nature Photonics* **3**, 206 (2009).
4. A. Blanco-Redondo, C. Husko, D. Eades, Y. Zhang, J. Li, T. F. Krauss, and B. J. Eggleton, *Nat. Commun.* **5**, 3160 (2014).
5. N. Ishikura, R. Hayakawa, R. Hosoi, T. Tamanuki, M. Shinkawa and T. Baba, *Appl. Phys. Lett.* **100**, 221110 (2012).
6. K. Kondo, and T. Baba, *Optica* **4**, 1109 (2017).
7. Y. Hinakura, H. Arai and T. Baba, *Opt. Express* **27**, 14321 (2019).
8. H. Ito, Y. Kusunoki, J. Maeda, D. Akiyama, N. Kodama, H. Abe, R. Tetsuya, and T. Baba, *Optica* **7**, 47 (2020).
9. N. Ozaki, Y. Kitagawa, Y. Takata, N. Ikeda, Y. Watanabe, A. Mizutani, Y. Sugimoto, and K. Asakawa, *Opt. Exp.* **15**, 7974 (2007).
10. C. Y. Lin, X. Wang, S. Chakravarty, B. S. Lee, W. Lai, and R. T. Chen, *Appl. Phys. Lett.* **97**, 183302 (2010).
11. S. A. Schulz, L. O'Faolain, D.M. Beggs, T. P. White, A. Melloni, and T. F. Krauss, *J. Opt.* **12**, 104004 (2010).
12. P. Pottier, M. Gnan, and R. M. De La Rue, *Opt. Exp.* **15**, 6569 (2007).
13. X. Ren, L. Feng, Z. Lin, Z. Zhou, and X. Deng, *Optik* **124**, 6606 (2013).
14. M. Askari, and A. Adibi, *Appl. Opt.* **52**, 5803 (2013).
15. Y. Terada, K. Miyasaka, K. Kondo, N. Ishikura, T. Tamura, and T. Baba, *Opt. Lett.* **42**, 4695 (2017).
16. J. Lu, and J. Vuckovic, *Opt. Exp.* **21**, 13351 (2013).
17. C. Qian, B. Zheng, Y. Shen, L. Jing, E. Li, L. Shen, and H. Chen, *Nat. Photonics* **14**, 383 (2020).
18. Y. Ha, Y. Guo, M. Pu, F. Zhang, X. Li, X. Ma, M. Xu, and X. Luo, *Opt. Express* **28**, 7943 (2020).
19. T. Asano, and S. Noda, *Nanophotonics* **8**, 2243 (2019).
20. R. Abe, T. Takeda, R. Shiratori, S. Shirakawa, S. Saito, and T. Baba, *Opt. Lett.* **45**, 319 (2020).
21. J. Kennedy, and R. C. Eberhart, in *IEEE Int. Conf. Neural Networks* **4**, 1942 (1995).
22. A. J. Nebro, J. J. Durillo, J. Garcia-Nieto, C. A. Coello Coello, F. Luna, and E. Alba, in *IEEE Computational Intelligence in Multi-Criteria Decision-Making (MCDM)*, 66 (2009).

Full References

1. T. F. Krauss, "Why we need slow light?," *Nat. Photonics* **2**, 448 (2008).
2. T. Baba, "Slow light in photonic crystals," *Nat. Photonics* **2**, 465 (2008).
3. B. Corcoran, C. Monat, C. Grillet, D. J. Moss, B. J. Eggleton, T. P. White, L. O'Faolain & T. F. Krauss, "Green light emission in silicon through slow-light enhanced third-harmonic generation in photonic-crystal waveguides," *Nature Photonics* **3**, 206 (2009).
4. A. Blanco-Redondo, C. Husko, D. Eades, Y. Zhang, J. Li, T. F. Krauss, and B. J. Eggleton, "Observation of soliton compression in silicon photonic crystals," *Nat. Commun.* **5**, 3160 (2014).
5. N. Ishikura, R. Hayakawa, R. Hosoi, T. Tamanuki, M. Shinkawa and T. Baba, "Photonic crystal tunable slow light device integrated with multi-heaters," *Appl. Phys. Lett.* **100**, 221110 (2012).
6. K. Kondo, and T. Baba, "On-chip autocorrelator using counter-propagating slow light in a photonic crystal with two-photon absorption photodiodes," *Optica* **4**, 1109 (2017).
7. Y. Hinakura, H. Arai and T. Baba, "64 Gbps Si photonic crystal slow light modulator by electro-optic phase matching," *Opt. Express* **27**, 14321 (2019).
8. H. Ito, Y. Kusunoki, J. Maeda, D. Akiyama, N. Kodama, H. Abe, R. Tetsuya, and T. Baba, "Wide beam steering by slow-light waveguide grating and prism lens," *Optica* **7**, 47 (2020).
9. N. Ozaki, Y. Kitagawa, Y. Takata, N. Ikeda, Y. Watanabe, A. Mizutani, Y. Sugimoto, and K. Asakawa, "High transmission recovery of slow light in a photonic crystal waveguide using a hetero group-velocity waveguide," *Opt. Exp.* **15**, 7974 (2007).
10. C. Y. Lin, X. Wang, S. Chakravarty, B. S. Lee, W. Lai, and R. T. Chen, "Wideband group velocity independent coupling into slow light silicon photonic crystal waveguide," *Appl. Phys. Lett.* **97**, 183302 (2010).
11. S. A. Schulz, L. O'Faolain, D.M. Beggs, T. P. White, A. Melloni, and T. F. Krauss, "Dispersion engineered slow light in photonic crystals: a comparison," *J. Opt.* **12**, 104004 (2010).
12. P. Pottier, M. Gnan, and R. M. De La Rue, "Efficient coupling into slow-light photonic crystal channel guides using photonic crystal tapers," *Opt. Exp.* **15**, 6569 (2007).
13. X. Ren, L. Feng, Z. Lin, Z. Zhou, and X. Deng, "Analysis of optical coupling between air-holes photonic crystal and tapered dielectric waveguides," *Optik* **124**, 6606 (2013).
14. M. Askari, and A. Adibi, "High efficiency coupling of light from a ridge to a photonic crystal waveguide," *Appl. Opt.* **52**, 5803 (2013).
15. Y. Terada, K. Miyasaka, K. Kondo, N. Ishikura, T. Tamura, and T. Baba, "Optimized optical coupling to silica-clad photonic crystal waveguides," *Opt. Lett.* **42**, 4695 (2017).
16. J. Lu, and J. Vuckovic, "Nanophotonic computational design," *Opt. Exp.* **21**, 13351 (2013).
17. C. Qian, B. Zheng, Y. Shen, L. Jing, E. Li, L. Shen, and H. Chen, "Deep-learning-enabled self-adaptive microwave cloak without human intervention," *Nat. Photonics* **14**, 383 (2020).
18. Y. Ha, Y. Guo, M. Pu, F. Zhang, X. Li, X. Ma, M. Xu, and X. Luo, "Minimized two- and four-step varifocal lens based on silicon photonic integrated nanoapertures," *Opt. Express* **28**, 7943 (2020).
19. T. Asano, and S. Noda, "Iterative optimization of photonic crystal nanocavity designs by using deep neural networks," *Nanophotonics* **8**, 2243 (2019).
20. R. Abe, T. Takeda, R. Shiratori, S. Shirakawa, S. Saito, and T. Baba, "Optimization of H0 photonic crystal nanocavity using machine learning," *Opt. Lett.* **45**, 319 (2020).
21. J. Kennedy, and R. C. Eberhart, "Particle Swarm Optimization," in *IEEE Int. Conf. Neural Networks* **4**, 1942 (1995).
22. A. J. Nebro, J. J. Durillo, J. Garcia-Nieto, C. A. Coello Coello, F. Luna, and E. Alba, "SMPSO: A New PSO-Based Metaheuristic for Multi-objective Optimization," in *IEEE Computational Intelligence in Multi-Criteria Decision-Making (MCDM)*, 66 (2009).